Wide-angle seismic profiling across an active rifted zone in the middle Izu-Ogasawara arc - KY0511 cruise -

Narumi Takahashi[1], Aki Ito[1], Shuichi Kodaira[1] and Yoshiyuki Kaneda[1]

Abstract We carried out a deep wide-angle seismic experiment using a large airgun array and total 110 ocean bottom seismographs (OBSs) in the middle Izu-Ogasawara arc area, which was conducted by R/V Kaiyo of Japan Agency for Marine-Earth Science and Technology (JAMSTEC) from October 5 to November 3, 2005 (KY05-11 cruise). Objectives of this cruise are to know a velocity structure of the across the northern Izu arc, especially velocity variation between an old Eocene arc beneath the forearc and a new active arc, and a relationship between the structural heterogeneity with the velocity variation and the active backarc rifting. These are important keys to clarify nature of the oceanic arc growth. An airgun-OBS seismic line was set from a trench slope break adjacent to the Izu-Ogasawara trench to the western Shikoku Basin through the forearc basin, the volcanic front, the Sumisu rift, the Miocene rear arc, the eastern Shikoku Basin and the Kinan seamount chain. We shot a large airgun array with total volume 12,000 cu. in. and recorded the seismic signals on OBSs with four components and a 24-channel hydrophone streamer. In this paper, we summarize information of the seismic experiments and introduce OBS data and reflection data.

Keywords: Crustal structure, seismic, wide-angle data, OBS, Izu-Ogasawara, backarc rifting

1. Introduction

The Izu-Ogasawara arc is typical oceanic island arc having andesitic middle crust with P-wave velocity 6 km/s (e.g., Suyehiro et al., 1996) and one of best examples to study continental growth. Because the andesitic oceanic island arc with relative light components has been produced from the oceanic crust with basaltic components through boninitic activities, the arc evolution study is comparable to know a process to remove heavy crustal components from the original crust.

The Izu-Ogasawara arc tectonic history is already known well from previous studies (e.g., Karig and Moore, 1975; Hall et al., 1995; Macpherson and Hall, 2001). At Eocene time, the initial island arc had been produced by subduction of the basaltic oceanic crust beneath the other basaltic oceanic crust. Then, the initial arc had developed there to Oligocene time. After the active rifting within the old arc, the Shikoku basin had spread during about 30-15 Ma (e.g., Okino et al., 1998) and the old arc had been divided two parts, which are the current Ogasawara ridge and the Kyushu Palau ridge, respectively (e.g., Hall et al., 1995). The volcanic activity within the arc during the opening of the Shikoku basin is still poorly understood, and had been activated again at the western adjacent region of the old arc at Miocene time (Taylor, 1992). The western area of the Izu-Ogasawara arc including en echelon seamount chain corresponds to the Miocene arc.

Here, we identify three scientific issues to be resolved considering above tectonics. These are (1) identification of the Eocene-Oligocene arc and the comparison with the Miocene arc and the current active arc based on a seismic structure, (2) relationship between the velocity variation and the rifting occurred behind the volcanic front and (3) the structure of the transition zone between the arc and the backarc. We summarize the objectives of this cruise and the background.

First objective is a continuity of the old Eocene-Oligocene arc. To understand nature of the crustal growth and estimate a crustal production rate, the geologic environment is important. It is clarified from petrologic studies that the Ogasawara ridge corresponds to the Eocene arc (e.g., Yuasa and Murakami, 1985) and the continuity is confirmed by only topographic fea-

1 Japan Agency for Marine-Earth Science and Technology

tures. ODP Leg 125 found that boninites widely distribute around the outer arc high of the northern Izu-Ogasawara arc (e.g., Pearce et al., 1992). From seismic velocity model, there is a difference in the velocity gradient of the middle crust between the current rifted zone and the forearc (Takahashi et al., 1998). However, it is still unknown that this velocity variation between the rifted zone and the forearc can be applied at whole of the Izu-Ogasawara arc. To confirm the commonality of the distribution of the velocity variation and the continuity of the Eocene arc is one of important keys to understand past crustal growth history.

Another objective is a role of the backarc opening for the crustal growth. The andesitic middle crust with P-wave velocity of 6 km/s was detected in the northern Izu-Ogasawara arc (Suyehiro et al., 1996, Takahashi et al., 1998) and the Tonga arc (Crowford et al.,2003), but not in the central and eastern Aleutian arc (Holbrock et al., 1999; Fliedner and Klemperer, 2000), nevertheless above all arcs are the same oceanic island arcs. So, a crustal growth model, which could explain such structural variation is needed. One candidate reason for the difference might be a degree of crustal growth. Recently, it is suggested that the velocity model of the Mariana arc-backarc system has advanced crustal growth area adjacent to the Mariana trough backarc basin (Takahashi et al., in Prep). Because the Izu-Ogasawara and the Tonga arcs have backarc basin and the central Aleutian arcs does not have, the backarc opening might be one of candidates to contribute to the crustal growth. The Sumisu rift is initial backarc basin, and it is possible that we can understand an influence of the backarc opening for the velocity structure. If rising magmas through the upper mantle are underplated beneath the Moho actively, the velocities of the lower crust and the upper mantle may have anomaly just beneath the Sumisu rift. If the backarc opening promotes the crustal growth, the velocity of the lower crust just beneath the Sumisu rift might be relatively slower than 7 km/s according to example of Mariana arc. Recently, Nishizawa et al. (2003) indicated that the velocity structure across the middle Izu-Ogasawara arc (30 degree north), however, the above influence of the velocity structure by the backarc opening was not detected due to lack of number of ocean bottom seismographs (OBSs). Understanding of the backarc opening at the initial stage is one of the targets in this study.

The other objective is velocity variation of the arc-backarc transition region. In particular, the lower crust with high velocity of over 7km/s at the arc-backarc transition region is reported frequently. The northern Izu-Ogasawara arc, the Mariana arc, the West Mariana ridge and the Tonga arc have such high velocity lower crust (Suyehiro et al., 1996; Takahashi et al., 2005; Crowford

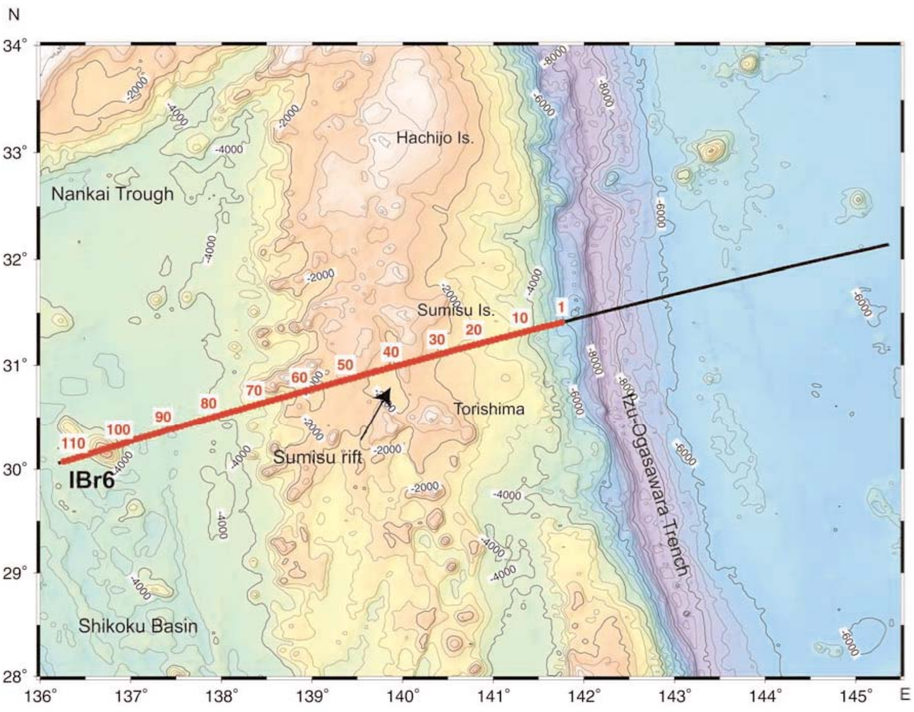

Figure 1: Map of the experimental area. Solid circles indicate OBSs. We shot an airgun array on a thick black line.

et al., 2003). The anomalous structure is detected well at the continental margin, and there are two processes to make the high velocity lower crust. One is underplated gabbroic complex beneath the Moho accompanied with the backarc opening as active margin (e.g., Berndt et al., 2001), and the other is serpentinite materials added to bottom of the crust during period between the rifting to the spreading as passive margin (e.g., Chain et al., 1995). According to this story, if the current eastern end of the Shikoku basin has the high velocity lower crust as passive margin, this means that there is a fragment of the Eocene-Oligocene old arc just before the backarc opening located at the position of the current western Izu-Ogasawara arc. However, Yamazaki and Yuasa (1998) indicated that the Miocene arc had been constructed on the past eastern end of the Shikoku basin, and Okino et al., (1994) also suggested that the past magnetic anomaly before the construction of the Miocene arc can be detected at the western Izu-Ogasawara arc. If such a high velocity lower crust is detected commonly along the western Izu-Ogasawara arc, it might indicate other tectonic story.

To clarify above objectives, we carried out the deep seismic profiling with 110 OBSs, a large airgun array and a 24-channel streamer along a line across the arc including the initial backarc region, the Sumisu rift, in the middle Izu-Ogasawara arc.

2. Experiments

We performed a wide-angle seismic profiling using 110 ocean bottom seismographs (OBSs), a large airgun array with capacity of 12,000 cubic inches and a 24-channel analogue streamer in middle Izu-Ogasawara arc (Figure 1). The period of this cruise using the R/V "Kaiyo" of Japan Agency for Marine-Earth Science and Technology (JAMSTEC) is from October 5 to November 3, 2005 (Figure 2). A main seismic line runs from a trench slope break neat the Izu-Ogasawara trench to the western Shikoku Basin through the forearc basin, the volcanic front, the Sumisu rift, the Miocene arc, the eastern Shikoku Basin and the Kinan seamount chain. We divided the main line into two parts, which are the eastern part from the trench slope break to the eastern edge of the Shikoku basin and the western part from the rift zone to the western Shikoku basin (Figure 3). The R/V Kaiyo departed from Yokohama shinko at October 5, and 77 OBSs deployment on the eastern part of the main line was carried out from October 6 to 9. We shot the airgun from October 10 to 12 on the eastern half (Line IBr6_obs_0). Then, after long standing by due to tottery typhoon attack, we recovered 46 OBSs deployed in eastern part during October 21 to 23. After we deployed 33 OBSs again on the western half to October 25, airgun shooting was carried out to October 27 (Line

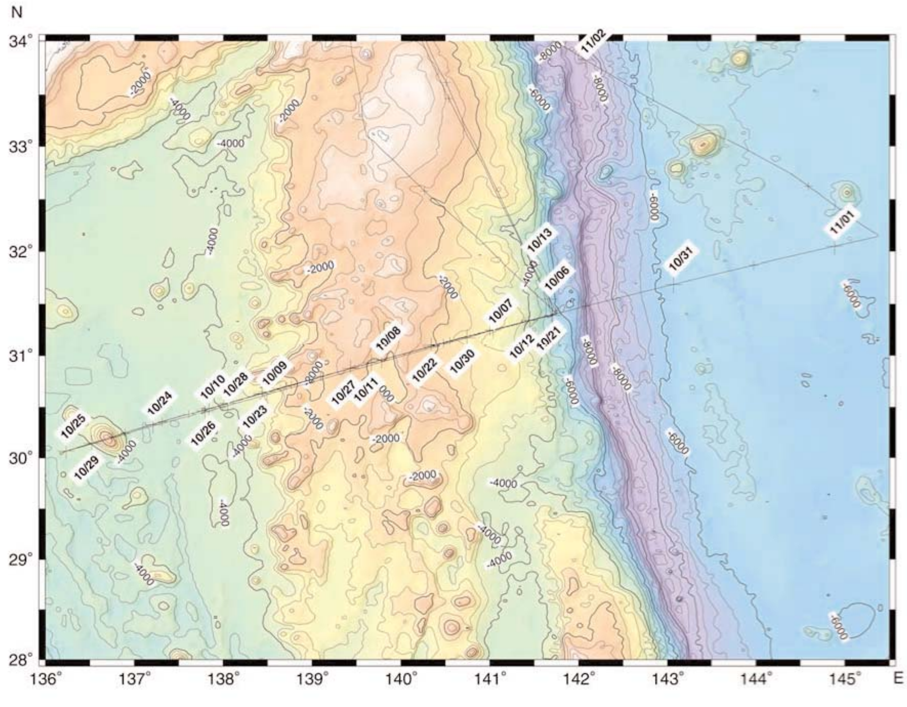

Figure 2: Map for ship's track line. Cross marks indicates ship position of every 6 hours.

IBr6_obs_1), and then we recovered 66 OBSs until October 30. An additional multichannel seismic survey with a 24-channel streamer was performed between October 30 and November 1 along an extended main line to east (Line IBr6_mcs_0). This aim is to clarify the crustal deformation of a subducting oceanic crust. Finally, we arrived at JAMSTEC at November 3. The actual activities are shown in Table 1 and Figure 2.

In this cruise, we performed OBS recorder test using different sampling rate and different dynamic range to investigate waveform distortion by digital conversion. As shown in 2.2 section, because we have two types of our OBS digital recorder, we deployed three OBSs at the same location on the forearc region (Site#21). One OBS has a 16 bit recorder with sampling rate of 100 Hz. Another has a 20 bit recorder with sampling rate of 100 Hz. The other has a 20 bit recorder with sampling rate of 250 Hz.

2.1 Airgun shooting

As above description, we shot the airgun array separately for the eastern half (Line IBr6_obs_0) and the western half (Line IBr6_obs_1). The overlap between the eastern and the western lines was about 150 km, because the offset of 150 km from the OBS should have refractions through the upper mantle. The airgun array with total capacity of 12,000 cubic inches consists of eight airguns (BOLT Technology Corporation, PAR Air Gun Model 1500LL) with 1,500 cubic inches capacity each. The gun array was shot with the shot interval of 200 m and the accuracy of the shot times was 1 msec. These guns were shot with the same timing within 2 msec. The gun depth was 10 m. The air pressure sent to the chamber was 2,000 psi. The geometry of the seismic experiment is shown in Figure 4. The two floats with two airguns each were deployed from port and starboard sides, respectively. The airgun array's size is 14 m length × 20 m width. Airgun's position was kept 134.5 m behind the ship position (distances from ship antenna to the stern, and from the stern to center of the airgun array, are 29.5 m and 105 m, respectively). The shot times was measured by a TrueTime system (TrueTime GPS time & frequency receive, MODEL XL-AK) using GPS signals and the accuracy was 1 nsec.

For the MCS survey with a 24-channel streamer along the extended main line to east, a small airgun array with total capacity of 3,000 cubic inches (two airguns with 1,500 cubic inches capacity each) was shot. The shot interval was 50 m. A length of the airgun array was 5.5 m. Other specification of the airgun shooting, for example, accuracy of shot timing, the gun depth and the air pressure, were the same to that of shooting with interval of 200 m .

Skyfix system was used as the differential global

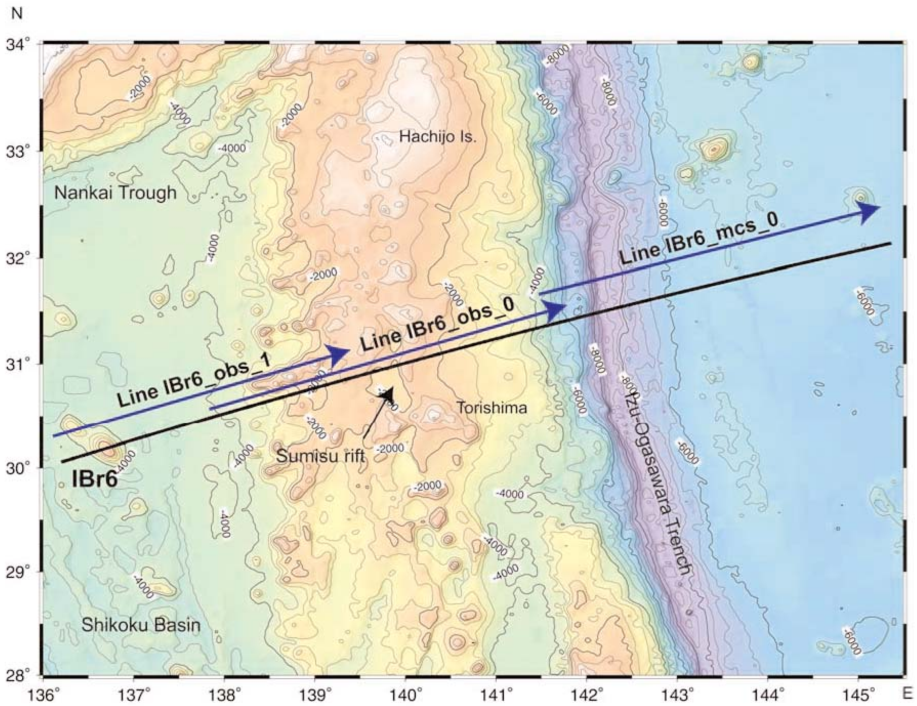

Figure 3: Map of airgun shooting. Blue arrows show a direction and a region of the shooting.

Table 1: Activity log during KY0511 cruise.

Date (UTC)	Remarks
October 05	Departure from Yokohama shinko
October 06	Transit and beginning OBS deployment on the eastern line (Site#1-Site#15)
October 07	OBS deployment (Site#16-Site#39)
October 08	OBS deployment (Site#40-Site#65)
October 09	Finish of OBS deployment (Site#66-Site#77)
October 10	Beginning IBr6_obs_0 airgun shooting on the eastern line
October 11	IBr6_obs_0 airgun shooting
October 12	Finish of IBr6_obs_0 airgun shooting and avoidance due to bad sea states
October 13	Avoidance due to typhoon attack
October 14	Avoidance due to typhoon attack
October 15	Avoidance due to typhoon attack
October 16	Avoidance due to typhoon attack
October 17	Avoidance due to typhoon attack
October 18	Avoidance due to typhoon attack
October 19	Avoidance due to typhoon attack
October 20	Transit and beginning OBS retrieval to Site#46 (Site#1)
October 21	OBS retrieval (Site#2-Site#28)
October 22	Finish of OBS retrieval (Site#29-Site#46)
October 23	Beginning OBS deployment on the western line (Site#78-Site#90)
October 24	Finish of OBS deployment (Site#91-Site#110)
October 25	IBr6_obs_1 airgun shooting on the western line
October 26	IBr6_obs_1 airgun shooting
October 27	Finish of IBr6_obs_1 airgun shooting and beginning OBS retreival (Site#47-Site#63)
October 28	OBS retreival (OBS#63-OBS#91)
October 29	OBS retreival (OBS#92-Site#110)
October 30	OBS#11 retrieval and beginning IBr6_mcs_0 airgun shooting
October 31	IBr6_mcs_0 airgun shooting
November 01	Finish of IBr6_mcs_0 airgun shooting and transit to JAMSTEC
November 02	Transit and arrived at JAMSTEC

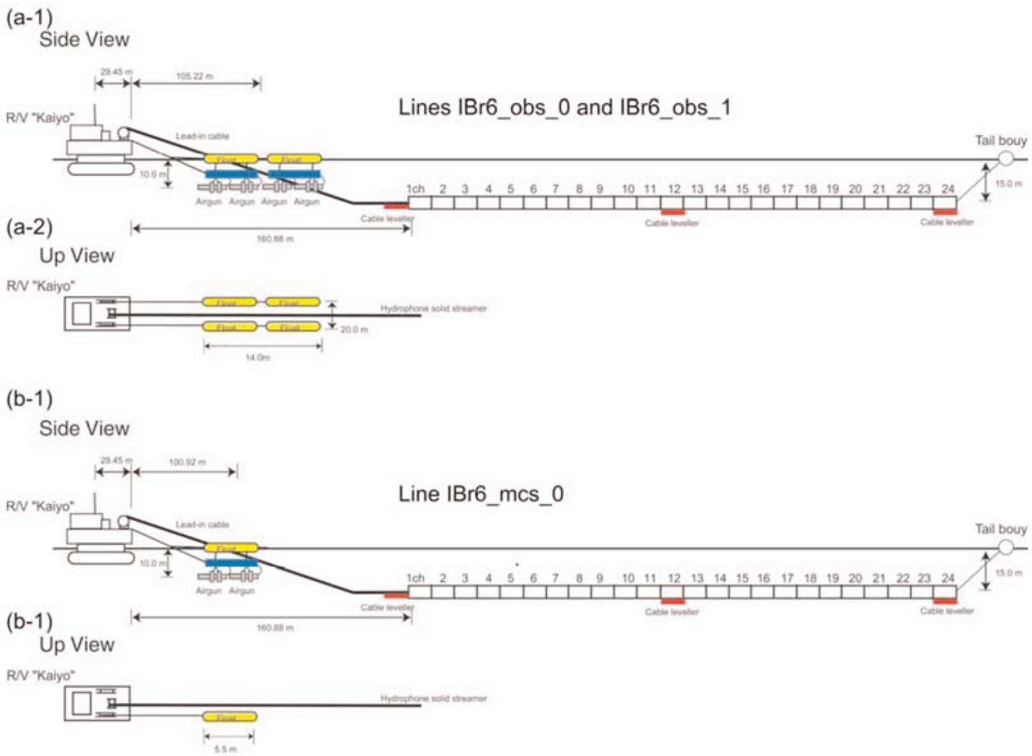

Figure 4: Side and up views for geometry of airgun system and the hydrophone streamer. (a) Lines IBr6_obs_0 and IBr6_obs_1. (b) IBr6_mcs_0.

positioning system (DGPS) of the R/V Kaiyo's navigation system. The base station was Naha, Okinawa, Japan. Because we have experienced the emergency stop of airgun shooting due to non-succession of GPS data in the past, we have adapted StarFire system as the seismic navigation system since 2004. Ship navigation system by Skyfix was used as backup of the seismic navigation system. The accuracy of shot position was about 40 cm.

2.2 Ocean Bottom Seismographs

We deployed 110 OBSs on the seismic line with the interval of 5 km (Figure 1, Table 3). Our seismic group in JAMTSEC has used 5 km as the OBS interval for the wide-angle seismic profiling carried out at the Izu-Ogasawara arc area to simplify comparison among the velocity models with the same resolution obtained along many seismic lines.

All OBSs were equipped with three-component geophones (vertical and two horizontal components perpendicular each other) using gimbal-leveling mechanisms and a hydrophone sensor. Natural frequency of these geophones was 4.5 Hz. The sensitivities of a geophone and hydrophone sensors are shown in Table 4. Our OBSs and the digital recorder system were originally designed by Kanazawa and Shiobara (1994) and Shinohara et al. (1993). The digital recorder used a 16-bit/20-bit A/D converter and stored data on digital audiotape or a hard disk sampling continuously with original format (Shinohara et al., 1993). The sampling rate is 10 msec. The electronic power for the recorder system of each OBS is supplied by rechargeable lithium-ion batteries. Above geophone sensors with gimbal-leveling mechanism, batteries and a recorder system are installed in 17-inch glass spheres made by Benthos, Inc, USA and Nautilus Marine Service GMGH, Germany. To enable easy OBS retrieval after arriving at sea surface, each OBS is attached to a flash light and a beacon with coded signals.

An OBS is deployed by free fall and retrieved by melting releaser composed of stainless steel plates connecting the OBS with a weight when a transponder system receives acoustic signal sent from a vessel. This acoustic communication between the OBS and the vessel was performed using transducers installed on the vessel. Positions of OBSs on sea bottom are estimated by SSBL of the vessels positioning system during the cruise. The accuracy of the OBS position determined by SSBL was about 100 m.

After the cruise, we edited the continuous OBS data with length of 70 sec and SEG-Y format. At the same time, the OBS clock was corrected by estimation of time differences between OBS original time and GPS time, which were measured immediately before OBS deployment and after OBS retrieval.

2.3 Multichannel hydrophone streamer

During airgun shooting, we towed a 24-channel hydrophone streamer to investigate the shallow structures, in particular, a distribution of sediments with low P-wave velocity and the fault configuration (Figure 4). Because one of the objectives of this cruise is to understand relationship between the velocity structure and the backarc opening, it is important to know the fault configuration within the Sumisu rift area. The hydrophone streamer (ITI, Stealtharray ST-48) cable is solid type and the interval of each channel was 25m. The lengths of active section and read-in cable from the stern are 600 m and 150 m, respectively, and a distance from the ship stern to near channel is 161 m. The streamer depth was 15 m. Hydrophone sensors (TYPE Bruel & Kjaer Free-field 1/2 Microphone) with sensitivity of -197.5 dB re 1Vµ Pa (13.3V/Bar) were used and analog signals from five sensors in the same channel were stacked before A/D conversion. The A/D conversion kit was attached in the recording system, the StrataVisor NX Marine made

Table 2: Airgun shooting log.

IBr6_obs_0	Time (UTC)	Latitude (N)	Longitude (E)	Depth (m)	SP
First shot	2005/10/10 0:39	30° 28.9902′	137° 49.9950′	4124	1964
First good	2005/10/10 0:39	30° 28.9902′	137° 49.9950′	4124	1964
Last good	2005/10/12 5:03	31° 25.3819′	141° 49.3926′		3940
Last shot	2005/10/12 5:03	31° 25.3819′	141° 49.3926′		3940

IBr6_obs_1	Time (UTC)	Latitude (N)	Longitude (E)	Depth (m)	SP
First shot	2005/10/25 2:00	30° 3.4256′	136° 12.1903′	4366	1145
shot	2005/10/25 2:00	30° 3.4256′	136° 12.1903′	4366	1145
Last good	2005/10/26 22:34	30° 53.2208′	139° 28.6550′	1520	2783
Last shot	2005/10/26 22:34	30° 53.2208′	139° 28.6550′	1520	2783

IBr6_mcs_hr	Time (UTC)	Latitude (N)	Longitude (E)	Depth (m)	SP
First shot	2005/10/29 6:15	31° 23.0232′	141° 38.6257′	5607	21405
shot	2005/10/29 6:21	31° 23.0759′	141° 38.9715′	5534	21416
Last good	2005/11/1 7:00	32° 8.4868′	145° 22.1362′	5787	
Last shot	2005/11/1 7:00	32° 8.4868′	145° 22.1362′	5787	

Table 3: OBS information. Each recorder using DAT or hard disk is shown by each abbreviation of D or "H". The "B" and "H" means that makers of the hydrophone sensor are Benthos Inc. and High Tech Inc., respectively.

		Coordinate			Estimated position by SSBL				Coordinate						
Site	Time UTC	Lat(N)	Lon(E)	Dep	Lat(N)	Lon(E)	Dep	Time UTC	Lat(N)	Lon(E)	Dep	Rec	A/D (bit)	Hyd	GS
1	10/6 1:10	31°24.4232'	141°45.1019'	5990	31°24.3804'	141°45.1384'	5991	10/20 23:01	31°24.2527	141°45.1742		H	16	B	U
2	10/6 2:56	31°23.7593'	141°42.0283'	5826	31°23.7375'	141°42.0319'	5831	10/21 0:10	31°22.9107	141°42.3381		H	16	B	U
3	10/6 4:35	31°23.0950'	141°38.9849'	5577	31°23.0230'	141°38.9204'	5583	10/21 0:59	31°22.7210	141°39.1275		H	16	B	U
4	10/6 6:10	31°22.4541'	141°35.9926'	5113	31°22.3740'	141°35.7995'	5125	10/21 2:41	31°22.1610	141°36.0316	5146	H	16	B	U
5	10/6 7:44	31°21.7807'	141°32.9729'	4668	31°21.7640'	141°32.8169'	4658	10/21 3:22	31°21.5623	141°33.0066	4694	D	16	B	U
6	10/6 9:12	31°21.0523'	141°29.8857'	4287	31°21.0587'	141°29.7630'	4285	10/21 4:40	31°20.9325	141°29.8728	4291	H	16	H	U
7	10/6 10:36	31°20.4257'	141°26.8614'	4125	31°20.4843'	141°26.7512'	4116	10/21 5:21	31°20.3867	141°26.8902	4111	H	20	B	U
8	10/6 12:03	31°19.6627'	141°23.7925'	3606	31°19.7640'	141°23.7753'	3604	10/21 6:09	31°19.6312	141°23.8470	3617	H	16	H	U
9	10/6 13:19	31°18.9436'	141°20.6436'	3448	31°19.0440'	141°20.6480'	3446	10/21 6:55	31°18.9227	141°20.7194	3446	H	16	B	U
10	10/6 14:35	31°18.2671'	141°17.5451'	3330	31°18.2885'	141°17.5583'	3317	10/21 7:43	31°18.1536	141°17.5467	3337	H	16	B	U
11_1	10/7 15:44	31°17.6219	141°14.5957	3324	31°17.7265	141°14.6387	3270	10/30 3:27	31°17.6758	141°14.8609	3306	H	16	B	U
11_2	10/6 18:36	31°17.7035'	141°14.5297'	3307	31°17.6842'	141°14.4773'	3326	10/21 8:29	31°17.5567	141°14.5264	3327	H	16	B	U
12	10/6 19:51	31°16.9947'	141°11.4611'	3211	31°17.0081'	141°11.3876'	3218	10/21 9:16	31°16.8820	141°11.4488	3209	D	16	B	U
13	10/6 21:02	31°16.2782'	141°08.5280'	2991	31°16.2482'	141°08.4145'	3001	10/21 10:01	31°16.1456	141°08.4723	2994	H	16	B	U
14	10/6 22:12	31°15.6667'	141°05.4714'	3022	31°15.6509'	141°05.2828'	3029	10/21 10:47	31°15.5752	141°05.3712	3024	H	16	B	U
15	10/6 23:19	31°14.9314'	141°02.3349'	3012	31°14.9578'	141°02.2463'	3028	10/21 11:31	31°14.9634	141°02.3424	3010	H	16	B	U
16	10/7 0:29	31°14.2422'	140°59.2525'	2965	31°14.2445'	140°59.1816'	2970	10/21 12:17	31°14.2898	140°59.2718	2961	H	16	B	U
17	10/7 1:34	31°13.5878'	140°56.2557'	2917	31°13.6269'	140°56.2209'	2913	10/21 13:02	31°13.7465	140°56.3378	2902	H	16	B	U
18	10/7 2:40	31°12.8362'	140°53.1355'	2803	31°12.9836'	140°53.0298'	2812	10/21 13:45	31°13.1560	140°53.1480	2803	H	16	B	U
19	10/7 3:46	31°12.1011'	140°50.1501'	2847	31°12.1504'	140°50.1141'	2857	10/21 14:34	31°12.4207	140°50.2161	2841	H	16	B	U
20	10/7 4:55	31°11.4972'	140°47.0604'	2807	31°11.5551'	140°47.1291'	2812	10/21 15:25	31°11.8344	140°47.2355	2740	H	16	B	U
21	10/7 6:02	31°10.8127'	140°44.0304'	2762	31°10.8396'	140°44.0065'	2773	10/21 16:10	31°11.2806	140°44.1819	2747	H	16	B	U
21-1	10/7 6:14	31°10.8051'	140°44.0098'	2754	31°10.8282'	140°43.9001'	2756	10/21 16:25	31°11.1113	140°44.0251	2738	H	20	B	U
21-2	10/7 6:17	31°10.7943'	140°44.0374'	2763	31°10.8174'	140°43.9391'	2759	10/21 16:54	31°11.1537	140°44.0627	2739	H	20	H	U
22	10/7 16:24	31°10.1323'	140°41.0656'	2679	31°10.1505'	140°40.9682'	2675	10/21 17:58	31°10.4845	140°41.1393	2658	H	16	B	U
23	10/7 17:30	31°09.4343'	140°38.0199'	2658	31°09.4678'	140°37.9093'	2646	10/21 18:49	31°09.7480	140°37.9683	2644	H	16	B	U
24	10/7 18:33	31°08.7378'	140°34.9673'	2519	31°08.7720'	140°34.8091'	2539	10/21 19:52	31°09.0444	140°34.8573	2539	H	16	B	U
25	10/7 19:34	31°08.0358'	140°31.9375'	2395	31°08.0928'	140°31.8838'	2401	10/21 20:48	31°08.3392	140°31.8596	2291	H	16	B	U
26	10/7 20:32	31°07.2775'	140°28.8924'	2214	31°07.3426'	140°28.8536'	2229	10/21 21:43	31°07.6494	140°28.8294	2239	H	16	H	U
27	10/7 21:27	31°06.5700'	140°25.8167'	2079	31°06.6649'	140°25.8588'	2075	10/21 22:39	31°06.8979	140°25.7816	2092	H	16	B	U
28	10/7 22:21	31°05.7982'	140°22.6388'	1985	31°05.9134'	140°22.7187'	1973	10/21 23:29	31°06.1510	140°22.6280	1991	H	16	B	U
29	10/7 23:11	31°05.1093'	140°19.6283'	1908	31°05.2235'	140°19.7461'	1895	10/22 0:22	31°05.4624	140°19.5943	1913	H	16	B	U
30	10/8 0:05	31°04.4201'	140°16.6087'	1804	31°04.4874'	140°16.7138'	1808	10/22 1:09	31°04.7070	140°16.6157	1808	H	20	B	U
31	10/8 1:01	31°03.7330'	140°13.5345'	1710	31°03.7887'	140°13.6037'	1737	10/22 1:56	31°03.9451	140°13.6133	1722	D	16	B	U
32	10/8 1:56	31°03.0373'	140°10.4886'	1574	31°03.0503'	140°10.6056'	1581	10/22 2:44	31°03.1984	140°10.6224	1573	H	16	B	U
33	10/8 2:51	31°02.3650'	140°07.4207'	1516	31°02.3508'	140°07.5078'	1522	10/22 3:32	31°02.5547	140°07.5732	1518	D	16	B	U
34	10/8 3:47	31°01.6664'	140°04.3848'	1479	31°01.6371'	140°04.4445'	1501	10/22 4:15	31°01.7019	140°04.6324	1486	D	16	B	U
35	10/8 4:39	31°00.9685'	140°01.3379'	1346	31°00.8432'	140°01.5002'	1353	10/22 5:08	31°00.8197	140°01.6069	1358	H	16	H	U
36	10/8 5:30	31°00.3060'	139°58.2557'	1122	31°00.2127'	139°58.2696'	1068	10/22 5:57	31°00.2422	139°58.3173	1065	D	16	B	U
37	10/8 6:16	30°59.6448'	139°55.3353'	1534	30°59.5690'	139°55.2903'	1573	10/22 7:00	30°59.5280	139°55.3006	1600	H	16	B	U
38	10/8 7:10	30°58.9222'	139°52.3352'	2278	30°58.8366'	139°52.3238'	2287	10/22 7:56	30°58.7858	139°52.2827	2273	D	16	B	U
39	10/8 8:12	30°58.2232'	139°49.3232'	2080	30°58.2111'	139°49.3611'	2072	10/22 8:53	30°58.0996	139°49.2963	2095	D	16	B	U
40	10/8 9:06	30°57.4739'	139°46.2567'	2018	30°57.4373'	139°46.2805'	2014	10/22 10:03	30°57.4091	139°46.2183	2034	H	16	H	U
41	10/8 10:02	30°56.7461'	139°43.2073'	2200	30°56.7061'	139°43.2227'	2214	10/22 11:02	30°56.6406	139°43.1788	2201	H	16	B	U
42	10/8 10:59	30°56.0379'	139°40.1858'	2197	30°55.9862'	139°40.2120'	2223	10/22 11:57	30°55.9431	139°40.1386	2218	H	16	B	U
43	10/8 11:56	30°55.3099'	139°37.1468'	2163	30°55.3631'	139°37.1864'	2179	10/22 12:56	30°55.2539	139°37.1452	2163	H	16	B	U
44	10/8 12:56	30°54.5180'	139°34.1256'	1493	30°54.5141'	139°34.1685'	1467	10/22 14:00	30°54.4274	139°34.1666	1489	H	16	B	U
45	10/8 13:47	30°53.7938'	139°31.0893'	1400	30°53.8005'	139°31.1269'	1438	10/22 14:44	30°53.8043	139°31.1613	1433	H	16	B	U
46	10/8 14:36	30°53.0675'	139°28.0653'	1556	30°53.0066'	139°28.0797'	1571	10/22 15:47	30°52.9891	139°28.1420	1578	H	20	B	U
47	10/8 15:28	30°52.3856'	139°25.0658'	1557	30°52.3252'	139°25.0716'	1567	10/27 0:24	30°52.3235	139°25.0376	1567	H	16	B	U
48	10/8 16:19	30°51.6171'	139°22.0015'	1512	30°51.5544'	139°21.9846'	1531	10/27 1:12	30°51.5287	139°21.9433	1523	H	16	B	U
49	10/8 17:10	30°50.9769'	139°19.0089'	777	30°50.9745'	139°19.0206'	778	10/27 1:56	30°50.9508	139°18.9771	762	H	16	B	U
50	10/8 17:48	30°50.1876'	139°15.9596'	1710	30°50.1012'	139°15.9070'	1739	10/27 2:42	30°50.1122	139°15.8686	1735	D	16	B	U
51	10/8 18:39	30°49.5205'	139°12.9523'	1936	30°49.4033'	139°12.8655'	1958	10/27 3:32	30°49.4167	139°12.8507	1939	D	16	B	U
52	10/8 19:32	30°48.8060'	139°09.9404'	1959	30°48.6413'	139°09.8763'	1967	10/27 4:22	30°48.6104	139°09.8403	1947	H	16	H	U
53	10/8 20:25	30°48.0350'	139°06.8910'	2011	30°48.0168'	139°06.8477'	2032	10/27 5:23	30°47.9656	139°06.8126	2015	H	16	B	U
54	10/8 21:19	30°47.2538'	139°03.8482'	2021	30°47.1945'	139°03.7339'	2035	10/27 6:04	30°47.1797	139°03.6946	2024	H	16	B	U
55	10/8 22:14	30°46.5380'	139°00.8782'	2006	30°46.5827'	139°00.8655'	2025	10/27 6:55	30°46.5746	139°00.8659	2008	H	16	B	U
56	10/8 23:10	30°45.7949'	138°57.8113'	1984	30°45.8383'	138°57.8423'	2007	10/27 7:44	30°45.8512	138°57.8769	1990	H	16	B	U
57	10/9 0:05	30°45.0433'	138°54.7988'	1853	30°45.0879'	138°54.8951'	1873	10/27 8:39	30°45.0679	138°54.9091	1873	H	16	B	U
58	10/9 1:00	30°44.3218'	138°51.7623'	1932	30°44.3649'	138°51.7989'	1951	10/27 9:30	30 °44.3228	138°51.5605	1938	D	16	H	U
59	10/9 1:57	30°43.5834'	138°48.7504'	2053	30°43.6261'	138°48.8112'	2069	10/27 10:19	30°43.5543	138°48.8491	2052	H	20	B	U
60	10/9 2:53	30°42.8293'	138°45.7252'	2190	30°42.8565'	138°45.7949'	2186	10/27 11:19	30°42.7480	138°45.7745	2192	H	16	B	U
61	10/9 3:50	30°42.0893'	138°42.7166'	2400	30°42.0964'	138°42.7580'	2403	10/27 12:17	30°41.9990	138°42.7179	2370	H	16	B	U
62	10/9 4:51	30°41.3520'	138°39.7022'	2451	30°41.3396'	138°39.7276'	2464	10/27 13:58	30°41.2233	138°39.5527	2448	H	16	H	U
63	10/9 5:53	30°40.6061'	138°36.6809'	2955	30°40.6119'	138°36.7480'	2949	10/27 15:00	30°40.5420	138°36.6079	2955	H	16	B	U
64	10/9 6:58	30°39.1636'	138°33.6575'	3116	30°39.8446'	138°33.6415'	3149	10/27 15:49	30°39.7399	138°33.5500	3130	D	16	B	U
65	10/9 8:06	30°39.1288'	138°30.6534'	3262	30°39.1389'	138°30.6721'	3284	10/27 16:38	30°39.0547	138°30.5617	3273	D	16	B	U
66	10/9 9:17	30°38.3774'	138°27.6395'	3396	30°38.4029'	138°27.6536'	3412	10/27 17:21	30°38.3179	138°27.6124	3396	D	16	B	U
67	10/9 10:30	30°37.6241'	138°24.6249'	3465	30°37.6451'	138°24.6239'	3471	10/27 18:08	30°37.5746	138°24.5792	3468	D	16	B	U
68	10/9 11:40	30°36.8816'	138°21.6157'	3429	30°36.8933'	138°21.5968'	3442	10/27 18:47	30°36.8057	138°21.6023	3430	H	16	B	U
69	10/9 12:52	30°36.1322'	138°18.6070'	3172	30°36.1466'	138°18.5787'	3181	10/27 19:37	30°36.0366	138°18.6233	3222	H	16	H	U
70	10/9 14:02	30°35.3702'	138°15.6434'	3752	30°35.3281'	138°15.5626'	3781	10/27 20:36	30°35.2711	138°15.6363	3754	H	16	B	U
71	10/9 15:15	30°34.6649'	138°12.6600'	3799	30°34.6296'	138°12.5880'	3809	10/27 21:26	30°34.6060	138°12.6376	3796	H	16	B	U
72	10/9 16:34	30°33.9165'	138°09.6807'	3869	30°33.9190'	138°09.5648'	3887	10/27 22:19	30°33.8650	138°09.6598	3871	D	16	B	U
73	10/9 17:50	30°33.1919'	138°06.6507'	3870	30°33.2204'	138°06.5034'	3882	10/27 23:01	30°33.1260	138°06.5868	3858	H	16	H	U
74	10/9 19:04	30°32.3627'	138°03.6048'	3644	30°32.3646'	138°03.4817'	3647	10/27 23:54	30°32.2761	138°03.5309	3632	H	16	B	U
75	10/9 20:14	30°31.6191'	138°00.6417'	3911	30°31.6686'	138°00.5671'	3924	10/28 0:26	30°31.9727	138°00.6239	3921	H	20	B	U
76	10/9 21:29	30°30.8610'	137°57.6275'	4042	30°30.8749'	137°57.5663'	4071	10/28 1:23	30°30.7584	137°57.7051	4044	H	16	B	U
77	10/9 22:45	30°30.1089'	137°54.6112'	4053	30°30.1002'	137°54.6131'	4085	10/28 2:05	30°29.9622	137°54.7163	4053	H	16	B	U
78	10/23 13:49	30°29.3563'	137°51.5209'	4120	30°29.3444'	137°51.5864'	4061	10/28 2:39	30°29.2536	137°51.5952	4121	H	16	H	U
79	10/23 15:18	30°28.5818'	137°48.5005'	4097	30°28.5777'	137°48.5735'	4053	10/28 3:39	30°28.4870	137°48.4799	4100	H	16	H	U
80	10/23 16:49	30°27.8326'	137°45.5551'	4078	30°27.8752'	137°45.5272'	4025	10/28 4:21	30°27.7940	137°45.4709	4079	H	16	B	U
81	10/23 18:16	30°27.0438'	137°42.5365'	4226	30°27.0705'	137°42.5665'	4166	10/28 5:20	30°27.0184	137°42.4623	4233	H	16	B	U
82	10/23 19:39	30°26.2751'	137°39.5301'	4262	30°26.3149'	137°39.5548'	4207	10/28 6:00	30°26.2595	137°39.4234	4258	H	16	B	U
83	10/23 21:03	30°25.5049'	137°36.3521'	4252	30°25.5246'	137°36.5526'	4188	10/28 6:55	30°25.5014	137°36.4144	4277	D	16	B	U
84	10/23 22:26	30°24.7538'	137°33.5319'	4247	30°24.7387'	137°33.6574'	4186	10/28 7:38	30°24.7091	137°33.5502	4250	H	16	H	U
85	10/23 23:51	30°23.9586'	137°30.5362'	4482	30°23.9294'	137°30.6337'	4414	10/28 8:39	30°23.8940	137°30.5251	4486	H	16	B	U
86	10/24 1:19	30°23.1962'	137°27.5355'	4469	30°23.1698'	137°27.6058'	4403	10/28 9:18	30°23.1540	137°27.5607	4471	H	16	B	U
87	10/24 2:44	30°22.4344'	137°24.5547'	4531	30°22.5287'	137°24.5343'	4460	10/28 10:21	30°22.3991	137°24.5700	4528	D	16	B	U
88	10/24 4:11	30°21.6460'	137°21.5503'	4516	30°21.6180'	137°21.5511'	4445	10/28 10:58	30°21.4457	137°21.5917	4513	D	16	B	U
89	10/24 5:38	30°20.8734'	137°18.5560'	4032	30°20.8344'	137°18.5492'	3987	10/28 12:07	30°20.6506	137°18.5380	4038	H	16	B	U
90	10/24 7:00	30°20.1175'	137°15.5562'	4305	30°20.1168'	137°15.5482'	4241	10/28 12:48	30°19.9333	137°15.4995	4335	D	16	B	U
91	10/24 8:20	30°19.3415'	137°12.5582'	4391	30°19.2677'	137°12.4656'	4336	10/28 13:43	30°19.1475	137°12.4078	4424	H	16	H	G
92	10/24 9:44	30°18.5757'	137°09.6545'	4444	30°18.5640'	137°09.5111'	4372	10/28 14:26	30°18.4519	137°09.4167	4460	D	16	H	G
93	10/24 11:10	30°17.7942'	137°06.5769'	4573	30°17.7802'	137°06.5230'	4500	10/28 15:20	30°17.6981	137°06.4020	4575	H	16	B	G
94	10/24 12:40	30°17.0104'	137°03.5731'	4486	30°17.0494'	137°03.4578'	4411	10/28 15:55	30°16.9707	137°03.3405	4466	H	16	B	G
95	10/24 14:04	30°16.2340'	137°00.6558'	4429	30°16.2109'	137°00.5936'	4361	10/28 16:55	30°16.1351	137°00.4269	4385	H	16	B	U
96	10/24 15:26	30°15.4701'	136°57.6693'	4329	30°15.4438'	136°57.6072'	4262	10/28 17:44	30°15.3653	136°57.4079	4323	H	16	B	U
97	10/24 16:44	30°14.6911'	136°54.7321'	4303	30°14.6528'	136°54.6430'	4247	10/28 18:27	30°14.5842	136°54.4842	4303	H	16	B	U
98	10/24 18:02	30°13.9169'	136°51.7183'	4118	30°13.8449'	136°51.6931'	4032	10/28 19:11	30°13.7706	136°51.5396	4085	H	16	B	U
99	10/24 19:16	30°13.1458'	136°48.7386'	3440	30°13.2037'	136°48.5920'	3325	10/28 19:59	30°13.1677	136°48.5037	3306	H	16	B	U
100	10/24 20:28	30°12.2608'	136°45.4568'	2144	30°12.2133'	136°45.4276'	2148	10/29 20:43	30°12.1329	136°45.1597	2140	H	16	B	U
101	10/24 21:30	30°11.4651'	136°42.4018'	905	30°11.4709'	136°42.3343'	898	10/29 21:24	30°11.4659	136°42.2915	931	H	16	H	U
102	10/24 22:08	30°10.7639'	136°39.7601'	1469	30°10.7510'	136°39.7160'	1471	10/28 22:11	30°10.7616	136°39.6732	1472	H	16	B	U
103	10/24 22:56	30°09.9229'	136°36.5742'	2673	30°09.9262'	136°36.5191'	2648	10/28 22:52	30°09.8984	136°36.4157	2708	H	16	B	U
104	10/24 23:54	30°09.1691'	136°33.7009'	3354	30°09.1884'	136°33.6208'	3317	10/28 23:34	30°09.1679	136°33.6026	3378	H	16	B	U
105	10/25 1:05	30°08.3746'	136°30.7321'	4071	30°08.3542'	136°30.6840'	4025	10/29 0:18	30°08.3264	136°30.6673	4085	H	16	B	U
106	10/25 2:25	30°07.5777'	136°27.7358'	4305	30°07.5136'	136°27.7542'	4236	10/29 1:03	30°07.4216	136°27.7348	4301	H	16	B	U
107	10/25 3:43	30°06.7824'	136°24.7538'	4391	30°06.7622'	136°24.7368'	4319	10/29 1:56	30°06.6815	136°24.6783	4391	H	16	B	U
108	10/25 5:06	30°05.9970'	136°21.7904'	4429	30°05.9528'	136°21.8142'	4363	10/29 2:37	30°05.8501	136°21.7739	4428	H	16	B	U
109	10/25 6:33	30°05.2215'	136°18.7563'	4079	30°05.1623'	136°18.6900'	4020	10/29 3:25	30°05.0739	136°18.6455	4050	H	16	B	U
110	10/25 7:51	30°04.4429'	136°15.9320'	4258	30°04.4633'	136°15.8051'	4197	10/29 4:09	30°04.3224	136°15.7082	4266	H	16	H	U

Table 4: Sensitivities of geophone and hydrophone sensors.

Sensor type	Sensor name	Maker	Sensitivity	Frequency
Geophone (three components)	L-28LB.H.V	Mark Products	0.69 V/in/sec	4.5Hz (natural freq.)
Hydrophone	AQ-18	Benthos, inc.	-169 dB	1Hz - 12kHz
Hydrophone	HTI-99DY	HIGH TECH, inc	-165dB	2Hz - 20kHz

by Geometrics Inc, and digitized data was recorded on DLT tapes with SEG-D 8048 4byte floating point format. System delay, which equals recording start time minus system start time, was 50 msec. The sampling rate was 4 msec and the record length was 13.5 sec. Because seismic records from fifth and sixteenth channels were not good during this cruise, we omitted the traces.

2.4 Seismic recording/shooting system

A seismic system of R/V Kaiyo consists of a navigation system with software SPECTRA, a recording system (StrataVisor NX Marine) and a gun controller system (GCS90), and these systems are connected via RTNμ as described by Takahashi et al. (2004). Navigation data collected from Starfire and Skyfix for the ship's navigation system was sent to the PC Linux machine installed SPECTRA software via the RTNμ. The Linux PC controls shot timing, assignment of shot number, and so on. Ship position (reference point of the vessel), shot time (sec), channel position estimated using cable leveler data and length of the read-in cable, water depth obtained by multi-narrow beam data system (Seabeam 2100 systrem), gun position, and shot number are stored with UKOOA P1/90 format. Added to above P1/90 format data, navigation data with interval of 1 sec, depth and direction of all cable leveler for all shots, gyrocompass data of the vessel, shot time received from GCS90 as time break signal (μ sec) and so on are stored with UKOOA P2/91 format. The system start signal generated by the SPECTRA was sent to the gun controller and the recording system as a trigger signal and the recording system started to store data on DLT tape. Then, the gun controller sends back the internal time break signal to the SPECTRA just after getting trigger signals. After 50 msec from arrival of system start signal to the gun controller, the trigger signals are sent to eight airguns as shot signals, and the recording system starts to record seismic data from a hydrophone streamer. It is reasonable to regard the time zero of recording start as just same timing to the gun fire.

3. Data

In this chapter, we introduce some representative examples of the seismic data obtained by OBSs and MCS. Vertical components of Site#13 on the forearc region, Site#35 near the volcanic front, Site#55 on the western side of the arc, Site#77 on the arc-backarc transition zone, and OBS#93 on the eastern Shikoku basin, and horizontal components of OBS#77 are described in Section 3.1. Multichannel sesimic data (MCS data) are described in section 3.2.

3.1 OBS

We retrieved all OBSs, however, recording system of one OBS had troubles. Almost data quality of available OBSs is basically good and we can trace the first phases on vertical records until 150-200 km distance from each OBS. Horizontal records also show good quality despite of poorer S/N ratio than the vertical, and we can see converted S arrivals until about 100 km from the OBS. We describe characteristics of OBS data using vertical record sections of Site#13 (Figure 5), Site#35 (Figure 6), Site#77 (Figure 7) and Site#93 (Figure 8) as follows.

OBS#13 was deployed on the eastern forearc region over the outer arc high. We can trace first phases to the western offset of 200 km from the OBS (Figure 5). The apparent velocities of the first phases in the eastern side are 2.5 km/s, 4.3 km/s, 6.5 km/s and 5.6 km/s for offsets of 3-7 km, 7-12 km, 12-28 km and over 28 km, respectively. The apparent velocity becomes small at the offset of 28 km due to the bathymetric change at the trench slope break. In the western side, we can trace them with apparent velocities of 3.3 km/s, 5.7 km/s, 7.2 km/s, 8.6 km/s and 8.0 km/s to offsets of 3-10 km, 10-20 km, 20-60 km except for 25-35 km, 60-100 km and over 130 km, respectively. Phases from the western side of over 130 km likely correspond to the refractions from the upper mantle (Pn). Severe variations of these apparent velocities at western offsets of 25-35 km and 100-130 km are due to topographic highs. Reflections from the Moho (PmP) with high amplitudes can be also seen at a western offset from 40 km. It is possible that a reflector with high amplitude at western offsets of 60-110 km indicates existence of a large faults developed within the arc.

OBS#35 was deployed near the volcanic front. The first phases could be traced 180 km (Figure 6). On the eastern side, we can trace first phases with apparent velocities of 3.0 km/s, 4.4 km/s, 5.7 km/s, 7.2 km/s and 7.8 km/s at offsets of 3-13 km, 13-20 km, 20-43 km, 43-

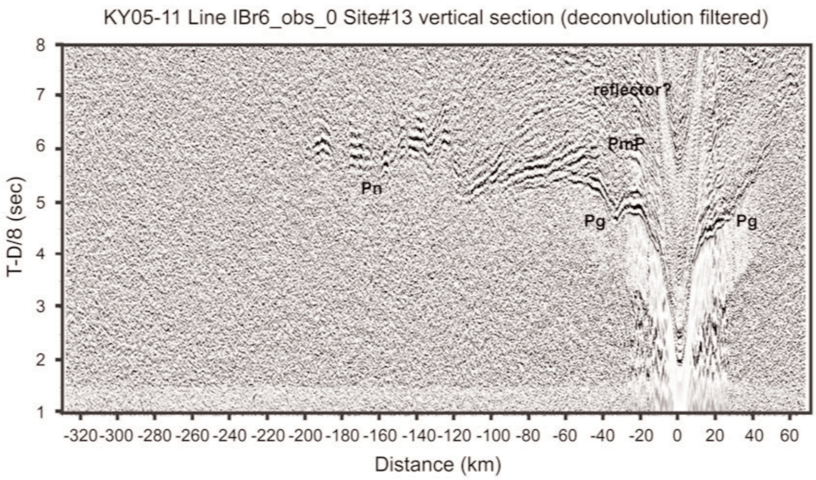

Figure 5: Vertical record section recorded by OBS#13. All traces are applied by deconvolution filter and the bandpass filter with 5-15 Hz. Vertical and horizontal axes are offsets (km) from OBS and traveltimes (sec) reduced by 8 km/s.

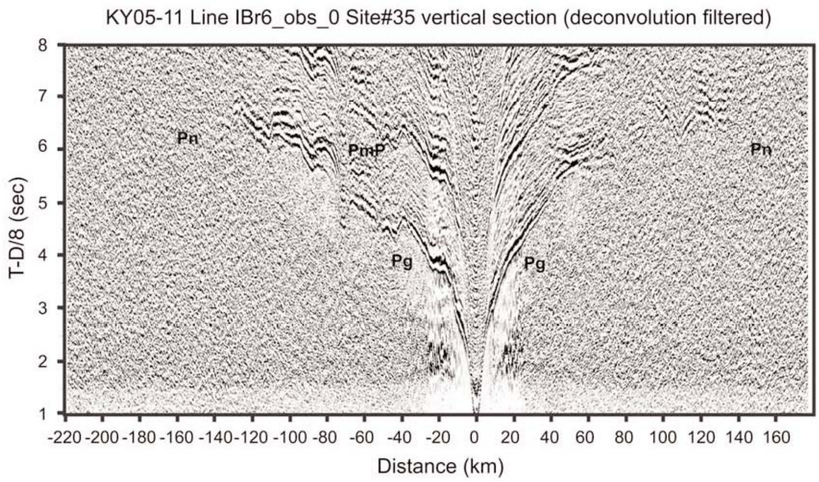

Figure 6: Vertical record section recorded by OBS#35. The details are same as for Figure 5.

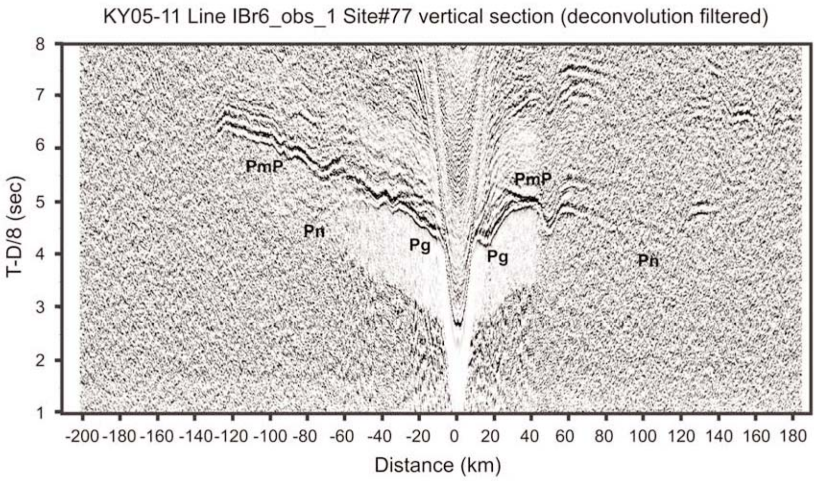

Figure 7: Vertical record section recorded by OBS#77. The details are same as for Figure 5.

55 km and over 55 km, respectively. In the western side, the apparent velocities of these phases are 3.4 km/s, 5.5 km/s, 6.3 km/s, 6.6 km/s and 7.8 km/s for offsets of 3-14 km, 24-40 km, 45-66 km and over 120 km, respectively. The phases with apparent velocity 7.8 km/s might correspond to the Pn. The PmP phases with high amplitudes can be seen at the western offset of 50-130 km.

OBS#77 was deployed on the arc-backarc transition zone. The first phases from distances of 100-150 km in both sides can be identified (Figure 7). In the eastern side, we can trace the first phases with apparent velocities of 2.2 km/s, 4.0 km/s, 7.2 km/s and 8.9 km/s for offsets of 3-5 km, 5-10 km, 23-35 km and 48-105 km, respectively. Two concave shapes at offsets of 10-23 km and 35-48 km are affected Miocene volcanoes at the western side of the arc. In the western side, the apparent velocity of the first phases are 2.5 km/s, 4.8 km/s, 6.3 km/s, 7.0 km/s and 8.6 km/s for offsets of 3-5 km, 5-10 km, 10-27, 27-37 km and over 37 km, respectively. Clear PmP phases identified at the eastern offsets of 15-55 km and the western offsets of 10-50 km indicate that the crustal thickness is relatively thinner than the arc.

OBS#93 was deployed on the eastern Shikoku basin. The first phases from distances of 120 km can be seen (Figure 8). In the eastern side, we can trace the first phases with apparent velocities of 5.3 km/s, 6.0 km/s, and 8.0 km/s for offsets of 5-10 km, 10-35 km and over 35 km, respectively. Small amplitude refractions with apparent velocity of 8.0 km/s possibly correspond to the Pn. High amplitude reflections identified at offsets of 30-85 km possibly corresponds to the PmP. In the western side, the apparent velocity of the first phases are 5.2 km/s and 7.1 km/s for offsets of 5-10 km and 10-26 km, respectively. Large concave shape seen at offsets of 26-65 km/s are affected by the Kinan seamount chain. Because the apparent velocity of first phases becomes over 8 km/s and the velocity corresponds to the Pn, thin crust is expected.

Above record sections indicate that the arc area has relative thick crust and the backarc area has thin crust. In particular, it is interesting that the arc-backarc area has relative thin crust despite the water depth is shallower than the typical oceanic crust. The high velocity lower crust beneath the arc-backarc transition zone or slow mantle velocity are expected. This is an important key to understand the crustal growth of this area.

Figures 9a and 9b indicate two horizontal components of OBS#77 crossing perpendicular with each other. Because only P-waves are shot in the sea, we have to observe phases converted from the P-wave to S-wave to understand S-wave structure. In the eastern side, we can see the converted S-waves with apparent velocities of 3.0 km/s and 5.0 km/s at offsets of 15-30 km and over 30 km, respectively. In the western side, the clear converted S-waves with apparent velocities of 3.8 km/s and 5.0-5.5 km/s were observed at offsets of 15-25 km and over 15 km, respectively.

3.2 MCS

The MCS data recorded by a 24-channel hydrophone streamer has enough quality to understand shallow fault configuration. The eastern part of MCS profile (Line IBr6_obs_0) and the western part (Line IBr6_obs_1) are shown in Figures 10 and 11. Applied tentative flows were a collection of spherical divergence, editing bad quality traces, a time variant filter (3-125 Hz), brute stacking of shot gather, a time variant bandpass filter of 20-50 Hz and the auto gain control. Because of the channel interval of 25m and the shot interval of 200 m, the fold number was 1 or 2.

Figure 10 indicates the MCS profile from the eastern part of the Izu-Ogasawara arc (Site#78) to near trench (5 km west from Site#1) and its interpretation. This part runs from the Miocene old arc at the arc-back arc transition area to the adjacent to the Izu-Ogasawara trench through the Sumisu rift (distance from the western end of the line: 340-375 km), the volcanic front (380 km), the forearc basin (385-510 km) and the trench slope break (510 km). Figure 11 indicates the MCS profile from the western side of the arc to the western Shikoku basin through the arc-back arc transition zone (130-260 km), the eastern Shikoku basin (70-240 km) and the Kinan seamount chain (30-70 km).

Uppermost sediments are deformed and collapsed. The deep reflections seen at about 10 sec might be corresponds to a top of the subducting oceanic crust. Beneath the forearc basin, the basement of the possible Eocene-Oligocene old arc with rough topography and thick sediments are remarkable characteristics. The basement traced continuously beneath the forearc is interrupted at the eastern adjacency of the volcanic front (410 km). We can see a thick sedimentary basin at the eastern half of the forearc region (460-490 km). This sedimentary basin is filled by three sequences and the lowest one likely pinches out at both ends of this basin. Because the sedimentary layer thickens toward the western part of the forearc, and because the internal interfaces incline toward east, these sedimentary layers is likely volcanoclastic materials from volcanoes located on the volcanic front.

The rift zone has the some seamounts and the small basins including the Sumisu rift. Inside the Sumisu

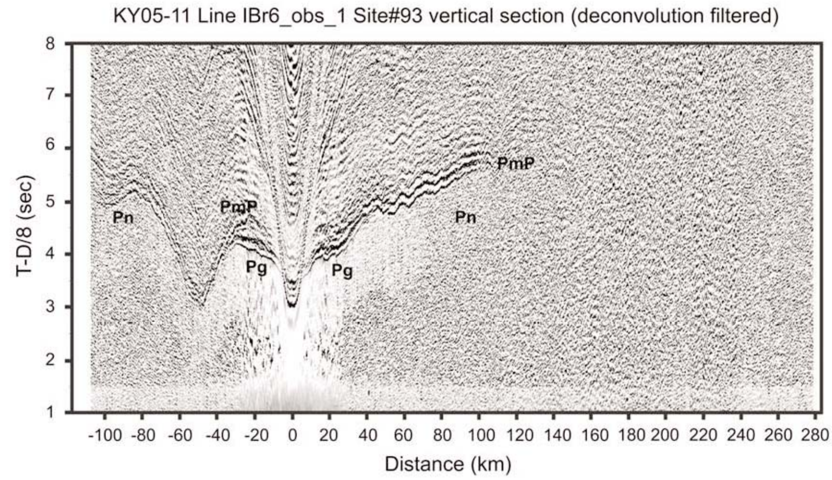

Figure 8: Vertical record section recorded by OBS#93. The details are same as for Figure 5.

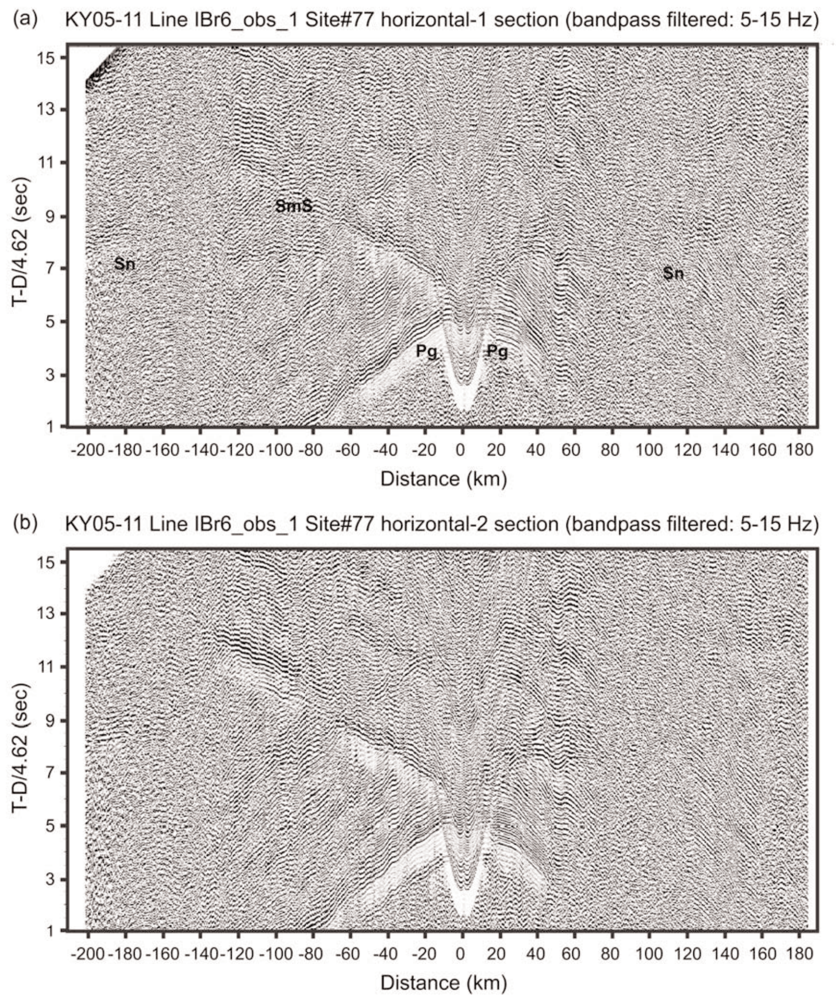

Figure 9: Horizontal record sections recorded by OBS#77. All traces are filtered by 5-15 Hz. The reduced velocity is 4.62 km/s. (a) Horizontal component-1. (b) Horizontal component-2.

rift, we can see some faults inclining toward east and a steep fault inclining toward west at the eastern edge of this rift. Some events with high amplitude also likely exist beneath the Sumisu rift. It is suggested that the initial backarc opening of this rift begins from forming asymmetric structure. At the western adjacent area of the Sumisu rift (295-335 km), events inclining toward east are detected. It might be speculated that the inclining events indicate existence of tilted block accompanied with the initial backarc opening. Between the distances of 270 km and 290 km, we can confirm a small basin bounded by intrusive seamounts.

In the arc-backarc transition zone, the water depth deepens gradually toward west. The height of seamounts lowers toward west. At the western side from distance of 200 km, seamounts and/or topographic high are covered with thick sediments. Sedimentary structure is also different between the eastern and the western sides in this area. The eastern side has relative thick sediments and the sedimentary structure consists of two or three layers. At the western side from 115 km distance, the sedimentary structure becomes simple with one acoustic transparency layer. The deeper events are also detected at depth of 8 sec and might correspond to the Moho.

The Kinan seamount chain consists of basaltic seamounts produced in last stage of the backarc opening (e.g., Okino et al., 1998). The seismic line goes across the summit of one of basaltic seamounts. The basement of the seamount in both sides has some terraces with the height of about 500-1500 msec. The seamount covered with the thin sediments has gentle and steep slope relating to the terraces of basement topography.

Line IBr6_mcs_0 runs from a trench slope break on the eastern forearc end to 145 degree east across a large transform fault. We can see the Moho interface at about 10 sec at western part of Figure 12. At east side from shot number of 26200, Moho interface indicates strong distortion changing the depth. We can confirm the severe topography at shot numbers between 27600 and 28200 and a normal and a reverse faults on western and eastern sides, respectively. The flower structure showing the transform components can not be seen, however, it look like that the fault configuration might indicate the slumping structure.

4. Summary

We carried out the large active seismics using 110 OBSs, a large airgun array with total capacity of 12,000 cubic inches and a 24-channel hydrophone streamer. Qualities of OBS and MCS data are good to understand the velocity structure and discuss the crustal growth in this area. The OBSs recorded clear phases to the offsets of 150-200 km from each OBS. A part of horizontal components of OBSs are also good and the converted S-waves could be recorded to the offsets of over 100 km. The OBS data suggests that the crustal thickness beneath the arc-backarc transition zone is relatively thin. The MCS data indicates the variation of the sedimentary structures, topography of the basement and the configuration of faults developed within the rift zone. We will construct the velocity model and understand structural variation suggesting crustal heterogeneity due to different age, the relationship between the crustal growth and the backarc opening, and structural characteristics of arc-backarc transition zone.

5. Acknowledgement

We greatly appreciate to following members of KY0511 cruise shipboard party described following, and would not be able to get succession of this seismic experiment without their efforts. We thank Dr. T. Tsuru, Dr. S. Miura, Dr. M. Yamashita, Dr. S. Sato and Dr. Y. Kaiho for planning discussion of this cruise and supporting during the cruise.

Marine technicians
Chief Technician Makoto Ito
Technician Hitoshi Tanaka
Technician Masato Sugano
Technician Ikumasa Terada
Technician Yuki Ohwatari
Technician Morifumi Takaesu
Technician Satoshi Okada
Technician Maiko Kimino
Technician Kimiko Serizawa
Technician Miho Ido
Technician Hiroyoshi Shimizu
Technician Yuko Yamakawa
Technician Suguru Inaba

Crew
Captain Osamu Yukawa
Chief Officer Koji Samejima
Second Officer Kazunori Kamiya
Junior Second Officer Akihisa Tsuji
Third Officer Jun Takao
Chief Engineer Hiroyuki Shibata
First Engineer Kazuhiko Kaneda
Second Engineer Saburo Sakaemura
Third Engineer Wataru Kurose
Chief Radio Officer Masamoto Takahashi
Second Radio Officer Kiyotaka Yamashita
Junior Second Radio Officer Kenji Takakusu

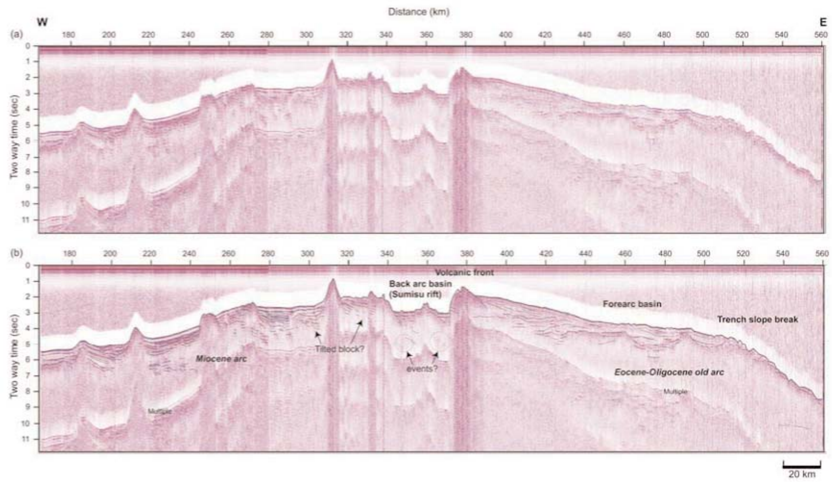

Figure 10: Eastern half of MCS profile (Line IBr6_obs_0). Horizontal axis is shot number (SP). (a) Stacked section (b) Interpretation.

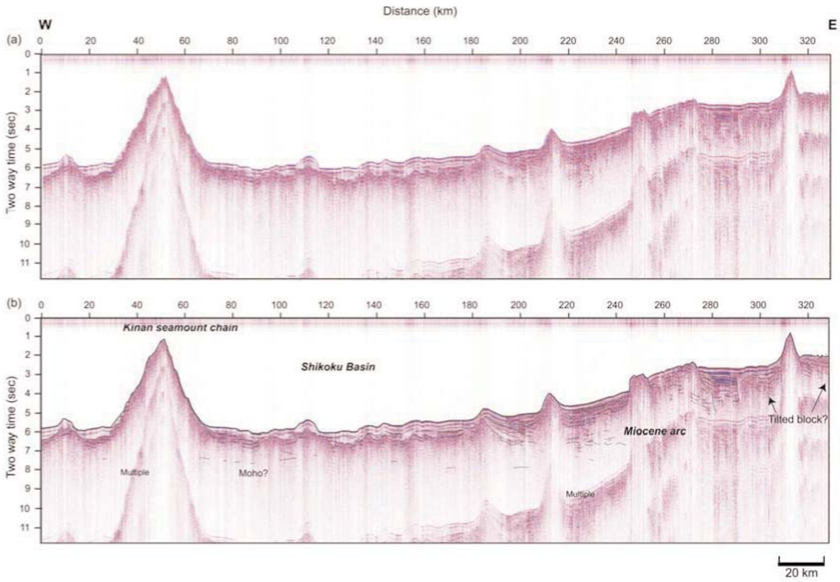

Figure 11: Western half of MCS profile (Line IBr6_obs_1). Horizontal axis is shot number (SP). (a) Stacked section (b) Interpretation.

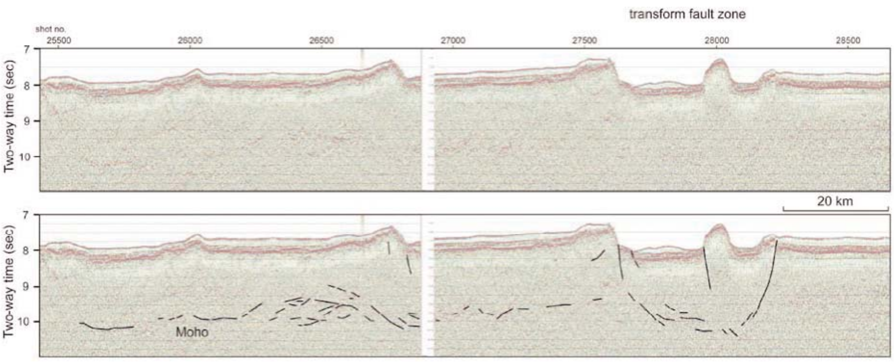

Figure 12: MCS profile along Line IBr6_mcs_0. Horizontal axis is shot number (SP). (a) Stacked section (b) Interpretation.

Boatswein Shoichi Abe
Able seaman Sakae Sasaki
Able seaman Tadahiko Taguchi
Able seaman Kinya Shoji
Able seaman Yasuo Konno
Able seaman Shuichi Yamamoto
Sailor Takumi Yoshida
No.1 Oiler Masayuki Masunaga
Oiler Kozo Miura
Oiler Hideo Hatakeyama
Oiler Takaatsu Inomoto
Assistant Oiler Keita Funawatari
Chief Steward Kyoichi Hirayama
Steward Tomohide Sonoda
Steward Yukio Tachiki
Steward Isao Matsumoto
Steward Hiroyuki Oba

References

1) Berndt, C., S. Planke, E. Alvestad, F. Tsikalas and T. Rasmussen, Seismic volcanostratigraphy of the Norwegian margin: constraints on tectonomagmatic break-up processes, J. Geol. Soc. London, 158, 413-426, (2001).
2) Chain, D., K. E. Louden and I. Reid, Crustal structure of the Labrador sea conjugate margin and implications for the formation of nonvolcanic continental margins, J. Geophys. Res., 100, 24239-24253, (1995).
3) Crawford, W. C., J. A. Hildebrand, L. M. Dorman, S. C. Webb, and D. A. Wiens, Tonga ridge and Lau basin crustal structure from seismic refraction data, *J. Geophys. Res., 108*, doi:10.1029/2001JB001435/2001JB001435, (2003).
4) Fliedner, M. M., and S. L. Klemperer, Crustal structure transition from oceanic arc to continental arc, eastern Aleutian islands and Alaska peninsula, *Earth Planet. Sci. Lett., 179*, 567-579, (2000)
5) Hall, R., J. R., Ali, C. D. Anderson, and S. J. Baker, Origin and motion history of the Philippine Sea Plate, *Tectonophysics, 251*, 229-250, (1995).
6) Holbrock et al., Structure and composition of the Aleutian island arc and implications for continental crustal growth, *Geology*, 27, 31-34, (1999).;
7) Kanazawa,T and H. Shiobara, Newly developed ocean bottom seismometer, Prog. Abst. Japan Earth and Planetary Science Meeting, 2, 240 (1994).
8) Karig, D. E. and G. F. Moore, Tectonic complexities in the Bonin arc system, *Tectonophysics*, 27, 97-118 (1975).
9) Macpherson, C. G. and R. Hall, Tectonic setting of Eocene boninite magmatism in the Izu-Bonin-Mariana forearc, *Earth Planet. Sci. Lett*., 186, 215-230 (2001).
10) Nishizawa, A., K. Kaneda, A. Nakanishi, N. Takahashi, and S. Kodaira, Crustal structure of the ocean-island arc transition at the mid Izu-Ogasawara (Bonin) arc margin, Earth Planets Space, 58, 8, e33-e36, (2006).
11) Okino, K., Y. Shimakawa, and S. Nagaoka, Evolution of the Shikoku basin, *J. Geomag. Geoelectr*., 46, 463-479, (1994).
12) Okino, K., S. Kasuga and Y. Ohara, A new scenario of the Parace Vela basin genesis, Mar. Geophys. Res., 20, 21-40 (1998).
13) Pearce, J. A., M. F. Thirlwall, G. Ingram, B. J. Murton, R. J. Arculus, and S. R. van der Laan, Isotope evidence for the origin of boninites and related rocks drilled in the Izu Bonin (Ogasawara) forearc, Leg 125, *Proc. ODP. Sci. Res., eds. Fryer, P., Pearce, J. A., Stokking, L., et al*., 125, 237-261, 1992.
14) Shinohara, M., K. Suyehiro, S. Matsuda and K. Ozawa, Digital recording ocean bottom seismometer using portable digital audio tape recorder. *J. Jpn. Soc. Mar. Surv. Tech*., 5, 21-31 (1993). (Japanese with English abstract)
15) Suyehiro, K., N. Takahashi, Y. Ariie, Y. Yokoi, R. Hino, M. Shinohara, T. Kanazawa, N. Hirata, H. Tokuyama, and A. Taira, Continental crust, crustal underplating, and low-Q upper mantle beneath an oceanic island arc, *Science*, 272, 390-392 (1996).
16) Takahashi, N., K. Suyehiro and M. Shinohara, Implications from the seismic crustal structure of the northern Izu-Ogasawara arc, *Island arc*, 7, 383-394 (1998).
17) Takahashi, N., S. Kodaira, S. Klemperer, Y. Tatsumi, Y. Kaneda and K. Suyehiro, Structure and evolution of Izu-Ogasawara (Bonin)-Mariana oceanic island arc crust, Geology, (in Prep).
18) Yamazaki, T. and M. Yuasa, Possible Miocene rifting of the Izu-Ogasawara (Bonin) arc deduced from magnetic anomalies, Island arc, 7, 374-382, (1998).
19) Yuasa, M., and F. Murakami, Geology and geomorphology of the Ogasawara arc and the Sofugan tectonic line, J. Geography, 94, 2, 47-66, 1985.

(Received July 13, 2006)